Chinese Chemical Letters 35 (2024) 108779

Contents lists available at ScienceDirect

Chinese Chemical Letters

journal homepage: www.elsevier.com/locate/cclet

Methyl functionalization of trimesic acid in copper-based metal-organic framework for ammonia colorimetric sensing at high relative humidity

Yuxin Wang[a], Zhengxuan Song[a], Yutao Liu[a], Yang Chen[a], Jinping Li[a], Libo Li[a,*], Jia Yao[b,*]

[a] College of Chemical Engineering and Technology, Shanxi Key Laboratory of Gas Energy Efficient and Clean Utilization, Taiyuan University of Technology, Taiyuan 030024, China

[b] Department of Gastroenterology, Shanxi Bethune Hospital, Shanxi Academy of Medical Sciences, Tongji Shanxi Hospital, Third Hospital of Shanxi Medical University, Taiyuan 030024, China

ARTICLE INFO

Article history:
Received 29 March 2023
Revised 6 June 2023
Accepted 5 July 2023
Available online 6 July 2023

Keywords:
Metal-organic framework
Ammonia sensing
Naked-eye color switching
High humidity
Respiration diagnosis

ABSTRACT

Exhaled ammonia (NH_3) can be used as a crucial biomarker of kidney and liver diseases. However, the high humidity in the detection conditions remains a challenge for accurate detection by gas sensors. Herein, a copper-based metal-organic framework (CH_3-Cu-BTC) with methyl (CH_3-) functionalization of trimesic acid was synthesized for NH_3 colorimetric sensing. The CH_3-Cu-BTC exhibited a strong response for 5 ppm NH_3 with high selectivity under high relative humidity (75% RH). Density functional theory (DFT) simulations indicated that the NH_3 molecules interacted more strongly with CH_3-Cu-BTC than H_2O molecules did, and the corresponding color switching was attributed to the lone-pair electron in NH_3 changing the coordination environment of Cu^{2+} ions, leading to an obviously visible color switching response from ruby green to blue. Based on the tailor-made pore chemistry, the precise detection of trace amounts of NH_3 in exhaled air was realized through functionalized MOF materials. The strategy used in this study not only offers a new pathway for the rapid detection of low concentration NH_3 under humid conditions, but also shows a method for early respiration diagnosis of kidney and liver diseases.

Ammonia (NH_3), a colorless gas with a pungent odor, in recent years, it has been confirmed to be a biomarker of kidney and liver diseases [1–3]. According to related report, the NH_3 amount in the exhaled air of healthy people is about 0.05–1.5 ppm [4–6], whereas that in the exhaled air of kidney patients is 0.8–15 ppm and liver patients is about 1.9–4.8 ppm [7–9]. Through accurate detection of the NH_3 concentrations will provide a non-invasive and convenient approach for early diagnosis of kidney diseases and for real-time physiological monitoring. In previous studies, NH_3 detection generally relied on device-complex electrochemical sensing [10–15], however, the high humidity in exhaled air (~90% relative humidity) has a significant impact on the sensitivity and veracity [16,17]. Thus, due to the requirements for rapid, simple and high humidity anti-interference, colorimetric sensing materials with naked-eye observation have gradually developed [18].

Among porous materials, benefiting from huge specific surface area [19,20], open metal sites [21–23], and designable frameworks [24–27], metal-organic frameworks (MOFs) have been extensively studied in the fields of gas sensing with naked-eye color switching [28,29]. In the past decade, researchers have realized the colorimetric sensing of NH_3 by adding chromophoric ligands in MOFs [30,31] or by transforming the metal center coordination environment [32,33]. Among them, FJU-56a demonstrates good selectivity and sensitivity for NH_3 sensing in competitive adsorption tests of H_2O and NH_3 [34]. Mn-BDC and SA/Co-MOF composite films show a noticeable color change on exposure to NH_3 and no color change when they are stored at 90% and 75% RH without NH_3 [35,36]. However, NH_3 detection at high humidity is still blank, which is because of the similar properties of H_2O and NH_3 molecules in terms of polarity and coordination, the competitive adsorption between H_2O and NH_3 will cause a remarkable influence on NH_3 sensing.

Hence, the main challenge in the real-time monitoring of the NH_3 content in exhaled breath is to find a balance between the selectivity and sensitivity of the NH_3 sensing MOF materials under high humidity conditions. We noticed that the Cu^{2+} ions of Cu-BTC would establish a discriminate strong interactions with NH_3, resulting in an obvious color switching, thus provided a feasible path

* Corresponding authors.
E-mail addresses: lilibo@tyut.edu.cn (L. Li), yaojia2006@163.com (J. Yao).

https://doi.org/10.1016/j.cclet.2023.108779
1001-8417/

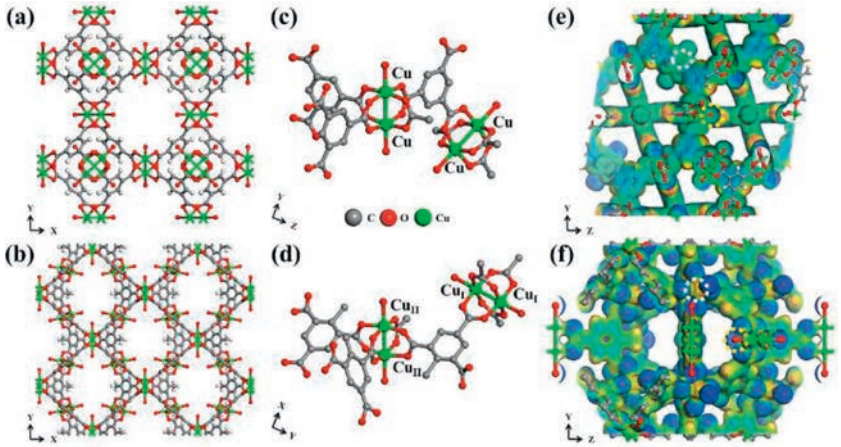

Fig. 1. Crystal structure of (a) Cu-BTC and (b) CH_3-Cu-BTC. Coordination environment of Cu atoms in (c) Cu-BTC and (d) CH_3-Cu-BTC. Electrostatic potential patterns of (e) Cu-BTC and (f) CH_3-Cu-BTC (blue-to-red colors indicate the high-to-low transition of electron density).

for low concentration NH_3 sensing [37,38]. And if methyl (CH_3-) functionalized organic linkers could precisely introduced in Cu-BTC that would change the distribution of electron clouds and improve the hydrophobicity of Cu-BTC, also strengthen nitrogen-containing species adsorption and show great selectivity for NH_3 in the co-adsorption of H_2O and NH_3 [39–42]. Herein, CH_3-Cu-BTC was constructed for a detailed study. Excitingly, compared to Cu-BTC, the introduction of CH_3- changes the topology (from tbo to fmj) and electron cloud density, and CH_3-Cu-BTC exhibits strong NH_3 detection ability with an excellent response for 5 ppm NH_3. In addition, the interaction with NH_3 molecules are able to changes the coordination environment of Cu^{2+} ions and causes color switching at high humidity conditions. Further, the electrostatic potential difference was identified by performing density functional theory (DFT) simulations, and the NH_3 molecules were determined to have stronger interactions than H_2O molecules with CH_3-Cu-BTC. Therefore, through a facile pretreatment, the precise detection of trace amounts of NH_3 in a patient's exhaled air was realized on the tailor-made MOF material, and this provides an innovative strategy for the early respiration diagnosis of kidney and liver diseases.

All reagents and solvents were obtained from commercial sources and used without further purification. CH_3-Cu-BTC was synthesized by the method reported previously [43].

Synthesis of CH_3-Cu-BTC: Copper nitrate trihydrate (72.48 mg, 0.3 mmol), methyl-1,3,5-benzenetricarboxylic acid (44.80 mg, 0.2 mmol), ethanol (3 mL), and deionized water (3 mL) were mixed in the Teflon reactor at 120 °C for 14 h, and then, ruby green crystals were obtained.

Powder X-ray diffraction (PXRD) patterns were collected on a Bruker D8 ADVANCE X-ray diffractometer using Cu Kα radiation. N_2 adsorption–desorption isotherms were recorded at 77 K on a Micromeritics ASAP 2460 instrument. Thermogravimetric analysis (TGA) was carried out in a N_2 atmosphere (N_2 flow rate: 100 mL/min) at a heating rate of 5 K/min using a TGA-50 (Shimadzu) thermogravimetric analyzer. Scanning electron microscopy (SEM) images were obtained using a Hitachi SU8010 scanning electron microscope. Fourier transform infrared spectroscopy (FT-IR) was performed using a Thermo Electron NEXUS 670. Ultraviolet-visible spectroscopy (UV–vis) was conducted using a Perkin-Elmer Model Lambda 650 spectrometer, with a $BaSO_4$ plate as the standard.

DFT calculations were used to identify the electrostatic potential difference and binding sites in CH_3-Cu-BTC. DFT calculations were employed using the Dmol3 and sorption module in Material Studio software. A semiempirical addition of dispersive forces to conventional DFT was included in the calculation to account for van der Waals interactions. During the DFT simulation, the structure of CH_3-Cu-BTC was first optimized, and then, the H_2O or NH_3 molecules were introduced to their potential locations in the MOF; this was followed by full structural relaxation.

The functionalization of MOF is accompanied by morphology changes: CH_3-Cu-BTC presents the fmj (orthorhombic crystal system) topology while Cu-BTC is the tbo (twisted boracite-type, cubic) topological structure (Figs. 1a and b). In the basic structural units of Cu-BTC and CH_3-Cu-BTC, each Cu ion forms coordination bonds with four oxygen atoms from carboxyl groups and a H_2O molecule bonds to the metal site (Figs. 1c and d). Further, two types of metal center were found in CH_3-Cu-BTC: Cu_I and Cu_{II} are linked to carboxyl groups located in the para- and ortho- positions of the methyl functional group, respectively. As shown in Figs. 1e and f, CH_3-Cu-BTC exhibits a much lower electron cloud density at Cu^{2+} sites and exhibits the distinct electron-rich (highlighted in yellow) and electron-poor sites (highlighted in white). These originate from the inductive effect and conjugative effect of CH_3- groups; thus, the Cu^{2+} sites are more accessible to accept the lone-pair electron in NH_3, which will change the metal center coordination environment and cause more sensitive color switching.

CH_3-Cu-BTC exhibited diamond-shaped octahedral crystals (Figs. S1a and b in Supporting information) though solvent thermal synthesis method, and the PXRD pattern of the CH_3-Cu-BTC powder was consistent with reported results (Fig. 2a) [43]. Through the test of FT-IR spectra on the CH_3-Cu-BTC powder, strong characteristic bands of CH_3-Cu-BTC were located at 1629 and 1377 cm^{-1} (Fig. 2b), corresponding to the stretching vibration of the C=O bond from the deprotonated trimesic acid and the stretching vibration of the C=C bond, respectively. To evaluate the porosity of CH_3-Cu-BTC, the as-synthesized samples were exchanged with ethanol several times and activated at 170 °C for 10 h under a high vacuum; then, the N_2 adsorption isotherms at 77 K around 1 atm were measured (Fig. 2c). The Brunauer-Emmett-Teller (BET) surface area was calculated as 1106 m^2/g, in agreement with previously reported results. The thermal stability of CH_3-Cu-BTC was investigated using TGA techniques, and the results showed that CH_3-Cu-BTC could be stable up to 300 °C under inert gas flow (Fig. 2d).

Benefiting from the strong binding affinity between Cu^{2+} ions and NH_3 molecules, CH_3-Cu-BTC is expected to be a good candidate for trace NH_3 colorimetric sensing. To explore the performance of CH_3-Cu-BTC for NH_3 detection, CH_3-Cu-BTC was exposed to ammonia vapor by the static volumetric method. Excitedly, the prepared CH_3-Cu-BTC showed different colors after exposure to

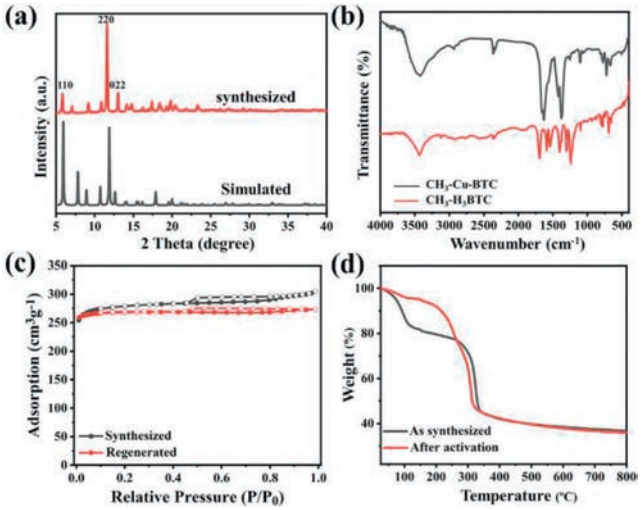

Fig. 2. (a) PXRD pattern of CH_3-Cu-BTC. (b) FT-IR spectra of CH_3-Cu-BTC and CH_3-H_3BTC. (c) N_2 sorption isotherms of as-synthesized and NH_3 regenerated CH_3-Cu-BTC at 77K. (d) TGA curves of CH_3-Cu-BTC under N_2 flow.

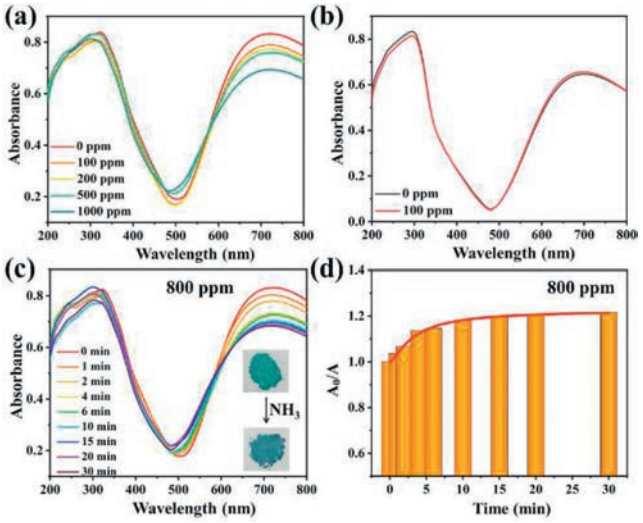

Fig. 3. (a) UV–vis DRS of CH_3-Cu-BTC after exposure to different NH_3 concentrations for 5 min. (b) UV–vis DRS of Cu-BTC before and after exposure to NH_3 (100 ppm) for 5 min. (c) UV–vis DRS of CH_3-Cu-BTC exposed to NH_3 for different periods. (d) A_0/A curve for different periods, where A_0 is the CH_3-Cu-BTC absorbance at 720 nm before exposure to NH_3, A is CH_3-Cu-BTC absorbance at 720 nm after exposure to NH_3.

different NH_3 concentrations, which could be further exploited in gas sensor applications due to the sensitive detection capability and visible color change.

Digital photographs clearly show the color switching that occurs on exposure to NH_3 with different concentrations: the color of CH_3-Cu-BTC changed from ruby green to blue in varying degrees (Fig. S2 in Supporting information). Fig. 3a shows the UV–vis diffuse reflectance spectra (UV–vis DRS) of CH_3-Cu-BTC after exposure to different NH_3 concentrations (100–1000 ppm). In this work, the absorbance of CH_3-Cu-BTC at 320 nm resulted from the CH_3-H_3BTC, whereas the higher absorbance at 650–750 nm was on account of the coordination of Cu^{2+} ions and CH_3-H_3BTC (Fig. S3 in Supporting information). The absorbance decreased obviously at 650–750 nm with increasing NH_3 concentration, which was because the coordination environment of Cu^{2+} ions changed with NH_3 adsorption. Furthermore, the absorbance of Cu-BTC after exposure to 100 ppm NH_3 barely differed from the original (Fig. 3b),

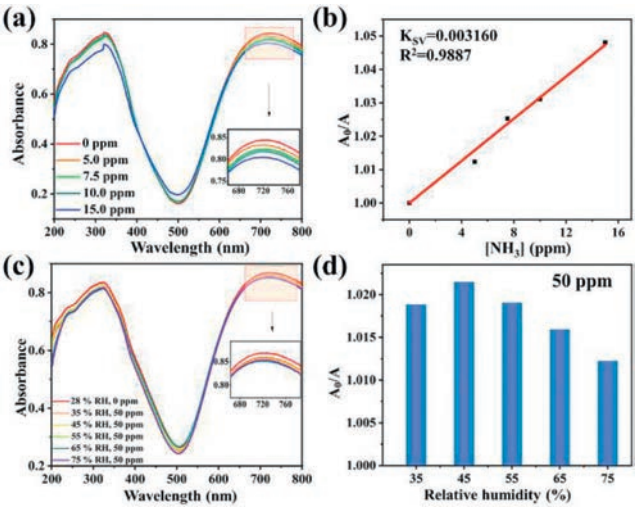

Fig. 4. (a) UV–vis DRS of CH_3-Cu-BTC after exposure to NH_3 with different concentrations. (b) A_0/A curve *versus* NH_3 concentrations. (c) UV–vis DRS of CH_3-Cu-BTC after exposure to 50 ppm NH_3 with different relative humidity. (d) A_0/A curve *versus* relative humidity.

which means that the CH_3- functionalization of Cu-BTC ligands greatly improves the NH_3 adsorption performance.

FT-IR spectra were used to verify the interaction between CH_3-Cu-BTC and NH_3, and a new double band at 3200 and 3350 cm^{-1} (bending vibration of the NH_2 group) was found when the sample was exposed to NH_3, indicating the strong combination between CH_3-Cu-BTC and NH_3 (Fig. S4 in Supporting information) [44,45]. Furthermore, the PXRD patterns and N_2 sorption of the CH_3-Cu-BTC powder adsorbed NH_3 and regenerated were compared, and the results show that the structure of the samples remain stable upon NH_3 adsorption (Fig. S5 in Supporting information and Fig. 2c). The morphology of CH_3-Cu-BTC also remains unchanged after NH_3 adsorption and desorption, demonstrating the stability of the material upon NH_3 adsorption (Figs. S1c-j in Supporting information).

The solid UV–vis DRS of CH_3-Cu-BTC in an NH_3 atmosphere were used to record the time-dependent color switching process at room temperature (30 °C) (Fig. 3c and Fig. S6 in Supporting information). The digital images show that the colors of CH_3-Cu-BTC differ between 0 and 30 min (illustration in Fig. 3c and Fig. S7 in Supporting information). Fig. 3d shows the color switching trend: the sample reacted immediately when contact with NH_3 was initiated and completed the color switching at 4 min. Here, A_0 is the CH_3-Cu-BTC absorbance at 720 nm before exposure to NH_3, and A is the CH_3-Cu-BTC absorbance at 720 nm after exposure to NH_3.

In order to identify the limit of detection of CH_3-Cu-BTC for NH_3 sensing, the solid UV–vis DRS of CH_3-Cu-BTC exposed to different NH_3 concentrations (0–15 ppm) were used to study the color switching process (Fig. 4a). Satisfactorily, the CH_3-Cu-BTC displayed a significant response toward NH_3 even when the concentration was decreased to 5 ppm. The plot of absorbance shifts at 720 nm with varying NH_3 concentrations is shown in Fig. 4b. The calculated K_{SV} is 0.003160 ppm^{-1} and R^2 is 0.9887, which are conform to the Stern-Volmer equation (Eq. 1) and comparable to the values for previously reported fluorescence and colorimetric NH_3 sensors [46,47].

$$(A_0/A) = K_{SV}[M] + 1 \quad (1)$$

Various NH_3 concentrations were created by the static volumetric method (Fig. S8 in Supporting information), which inevitably involved water vapor in the device. To exclude the influence of H_2O molecules and evaluate the selectivity, CH_3-Cu-BTC was ex-

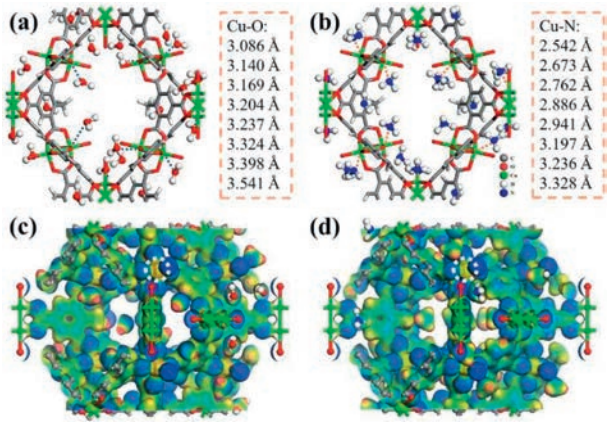

Fig. 5. (a) H_2O and (b) NH_3 adsorption sites in CH_3-Cu-BTC identified using DFT calculations. Change in electrostatic potential patterns of CH_3-Cu-BTC after the adsorption of (c) H_2O or (d) NH_3.

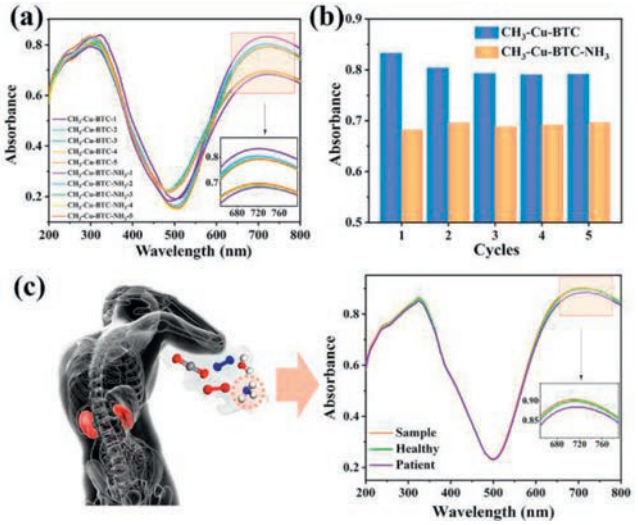

Fig. 6. (a, b) Response to NH_3 (800 ppm) during five cycles of adsorption and desorption. (c) UV–vis DRS of CH_3-Cu-BTC after exposure to patient's exhaled air and non-patient's exhaled air.

posed to high humidity conditions (75% RH) without NH_3. The UV–vis DRS clearly showed that the sample remained almost unchanged on exposure to water vapor (Fig. S9 in Supporting information), which demonstrated that the color response can be almost entirely attributed to NH_3 rather than to H_2O. The UV–vis DRS of CH_3-Cu-BTC exposed to 50 ppm NH_3 with different relative humidity were used to determine the selectivity (Fig. 4c). As shown in Fig. 4d, the absorbance of the sample remains largely unchanged when the relative humidity reaches up to 55%, and still exhibited obvious response even the relative humidity increased to 75%. The absorbance decrease at 75% RH can be attributed to a large amount of H_2O molecules significantly blocking the interaction between NH_3 and Cu^{2+} ions, and the kinetic diffusion of NH_3 molecules (Fig. S10 in Supporting information). Compared with other reported MOF for NH_3 sensing with naked-eye color switching, CH_3-Cu-BTC demonstrates excellent performance for the trace NH_3 detection under high humidity conditions (Fig. S11 in Supporting information).

DFT simulations were used to further study the thermodynamic affinities of H_2O and NH_3 to CH_3-Cu-BTC. In order to clearly identify the adsorption sites, H_2O and NH_3 molecules were introduced into the structure separately. As expected, after the adsorption equilibrium was reached, both molecules exhibited a binding affinity toward the Cu^{2+} ions. The distance between NH_3 and Cu^{2+} ions was shorter than that between H_2O and Cu^{2+} ions, which indicated that NH_3 had a stronger interaction with the Cu^{2+} ions (Figs. 5a and b). In addition, NH_3 also showed a lower binding energy (−45.10 kJ/mol) than H_2O (−34.56 kJ/mol).

To prove that the color switching is caused by changing the coordination environment of the Cu^{2+} ions, DFT calculations were performed to determine the electrostatic potential of the CH_3-Cu-BTC adsorbed H_2O and NH_3. As shown in Fig. 5c, after H_2O adsorption, the electrostatic potential of the Cu^{2+} ions remains almost unchanged (highlighted in white), indicating that H_2O molecules do not affect the coordination environment of metal sites and thus do not cause color switching of CH_3-Cu-BTC. However, as shown in Fig. 5d, after NH_3 adsorption, the electrostatic potential of the Cu^{2+} ions changes significantly, indicating the stronger interaction between NH_3 and Cu^{2+} ions and the transformation of the coordination environment in CH_3-Cu-BTC. Thus, according to the calculation results, NH_3 molecules show obvious advantage in the competitive adsorption at high humidity conditions, which will confirm the former color switching.

To investigate the stability of CH_3-Cu-BTC, PXRD tests were performed with the MOF powder exposed to air for different durations. The PXRD patterns demonstrated that the crystallinity and framework integrity of CH_3-Cu-BTC could be preserve at the room conditions for 1 month (Fig. S12 in Supporting information). In reversibility and durability tests, the absorbance changes for CH_3-Cu-BTC during five cycles of NH_3 (800 ppm) adsorption and desorption were analyzed on the basis of UV–vis DRS (Fig. 6a). As evidence in Fig. 6b, regenerated CH_3-Cu-BTC was obtained through heating at 60 °C for 30 min under high vacuum, and over 90% absorbance was maintained after the five continuous cycles, demonstrating the good stability and regenerability of CH_3-Cu-BTC for NH_3 sensing.

Because of the excellent selectivity and sensitivity, CH_3-Cu-BTC has great potential for exhaled breath detection of liver and kidney disease. Exhaled air for our respiration analysis was obtained from the Department of Gastroenterology, Shanxi Bethune Hospital. The UV–vis DRS of CH_3-Cu-BTC after exposure to a patient's and a healthy person's exhaled air were analyzed (Fig. 6c). Excitingly, a significant response was obtained for the patient's exhaled air, while hardly any difference was observed for the healthy person's exhaled air sample. Through linear equation calculations, the NH_3 concentration of the patient's exhaled air was found to be 6.3 ppm, while that of the non-patient was 0.9 ppm. In addition, selectivity test effectively demonstrated that color switching is largely attributed to NH_3 in the exhaled air (Fig. S13 in Supporting information). These results provide strong evidence of the potential of using this MOF material for the noninvasive early diagnosis of kidney and liver diseases, with the feasibility and efficiency being significantly better than those of traditional ammonia blood test.

In summary, through the target introduction of CH_3- functionalization ligands, we achieved the direct synthesis of CH_3-Cu-BTC and prepared an efficient material for NH_3 colorimetric sensing. With the tailor-made pore environment, CH_3-Cu-BTC displayed excellent performance for trace NH_3 sensing with visible color change, and demonstrated outstanding characters for NH_3 sensing under high humidity conditions. The stronger and selective interactions of CH_3-Cu-BTC with NH_3 molecules over H_2O molecules were clearly determined by DFT simulations, and the color switching is attributed to the change in the coordination environment of Cu^{2+} ions as a result of NH_3 adsorption. Benefiting from the optimized pore chemistry of CH_3-Cu-BTC, it can enable the quantitative detection of NH_3 in the air exhaled by patients with kidney and liver diseases. Thus, this work not only presents an effective solution for

trace NH_3 detection at high relative humidity, but also offers a feasible and efficient strategy for noninvasive diagnosis of kidney and liver diseases.

Declaration of competing interest

There are no conflicts to declare.

Acknowledgments

We gratefully acknowledge the financial support from the National Natural Science Foundation of China (Nos. 22090062, 22278287, 22278288), the Shanxi Province 136 Revitalization Medical Project (General Surgery Department), the Shanxi Provincial Guiding Science and Technology Special Project (No. 2021XM42), and the Basic Research Program of Shanxi Province (No. 202103021224341).

Supplementary materials

Supplementary material associated with this article can be found, in the online version, at doi:10.1016/j.cclet.2023.108779.

References

[1] L. Liu, T. Fei, X. Guan, et al., Sens. Actuator. B: Chem. 320 (2020) 128318.
[2] P.Le Maout, J.L. Wojkiewicz, N. Redon, et al., Sens. Actuator. B: Chem. 274 (2018) 616–626.
[3] Y. Su, G. Chen, C. Chen, et al., Adv. Mater. 33 (2021) 2101262.
[4] P. Španěl, S. Davies, D. Smith, et al., Rapid Commun. Mass Spectrom. 12 (1998) 763–766.
[5] C. Turner, P. Španěl, D. Smith, Physiol. Meas. 27 (2006) 321–337.
[6] T. Hibbard, A.J. Killard, Crit. Rev. Anal. Chem. 41 (2011) 21–35.
[7] S. Davies, P. Spanel, D. Smith, Kidney Int. 52 (1997) 223–228.
[8] Z.H. Endre, J.W. Pickering, M.K. Storer, et al., Physiol. Meas. 32 (2011) 115–130.
[9] S.T. Krishnan, J.P. Devadhasan, S. Kim, Anal. Bioanal. Chem. 409 (2017) 21–31.
[10] H. Zhao, L. Liu, X. Lin, et al., ACS Sens. 5 (2020) 346–352.
[11] Y. Liu, B. Sang, H. Wang, et al., Chin. Chem. Lett. 31 (2020) 2109–2114.
[12] H. Yuan, N. Li, W. Fan, et al., Adv. Sci. 9 (2022) 2104374.
[13] Y. Li, N. Luo, W. Zhang, et al., J. Mater. Chem. C 8 (2020) 12418–12426.
[14] Y. Lin, W. Li, Y. Wen, et al., Angew. Chem. Int. Ed. 60 (2021) 25758–25761.
[15] W. Zhang, J. Zhao, C. Cai, et al., Adv. Sci. 9 (2022) 2203428.
[16] A.W. Jones, Clin. Sci. 63 (1982) 441–445.
[17] A.H. Assen, O. Yassine, O. Shekhah, et al., ACS Sens. 2 (2017) 1294–1301.
[18] Z. Qiu, Y. Xue, J. Li, et al., Chin. Chem. Lett. 32 (2021) 2807–2811.
[19] H. Furukawa, N. Ko, Y.B. Go, et al., Science 329 (2010) 424–428.
[20] J. Li, J. Kuppler, H. Zhou, Chem. Soc. Rev. 38 (2009) 1477–1504.
[21] E.D. Bloch, W.L. Queen, R. Krishna, et al., Science 335 (2012) 1606–1610.
[22] L. Li, R. Lin, R. Krishna, et al., Science 362 (2018) 443–446.
[23] L. Dong, L. Zhang, J. Liu, et al., Angew. Chem. Int. Ed. 59 (2020) 2659–2663.
[24] P. Liao, N. Huang, W. Zhang, et al., Science 356 (2017) 1193–1196.
[25] A. Cadiau, K. Adil, P.M. Bhatt, et al., Science 353 (2016) 137–140.
[26] N. Li, R. Feng, J. Zhu, et al., Coord. Chem. Rev. 375 (2018) 558–586.
[27] X. Cui, K. Chen, H. Xing, et al., Science 353 (2016) 141–144.
[28] Y. Feng, Y. Wang, Y. Ying, Coordin. Chem. Rev. 446 (2021) 214102.
[29] H. Li, S. Zhao, S. Zang, et al., Chem. Soc. Rev. 49 (2020) 6364–6401.
[30] Q. Sui, P. Li, N. Yang, et al., ACS Appl. Mater. Interfaces 10 (2018) 11056–11062.
[31] B. Tan, C. Chen, L. Cai, et al., Inorg. Chem. 54 (2015) 3456–3461.
[32] A. Gładysiak, T.N. Nguyen, J.A.R. Navarro, et al., Chem. Eur. J. 23 (2017) 13602–13606.
[33] S. Sotirov, S. Demirci, M. Marudova, et al., IEEE Sens. J. 22 (2022) 3903–3910.
[34] J. Zhang, J. Ouyang, Y. Ye, et al., ACS Appl. Mater. Interfaces 10 (2018) 27465–27471.
[35] P. Goel, S. Singh, H. Kaur, et al., Sens. Actuator. B: Chem. 329 (2021) 129157.
[36] S. Feng, Q. Tang, Z. Xu, et al., Food Hydrocoll. 135 (2023) 108193.
[37] S. Xiang, W. Zhou, J.M. Gallegos, et al., J. Am. Chem. Soc. 131 (2009) 12415–12419.
[38] G.W. Peterson, D.K. Britt, D.T. Sun, et al., Ind. Eng. Chem. Res. 54 (2015) 3626–3633.
[39] P.Z. Moghadam, D. Fairen-Jimenez, R.Q. Snurr, J. Mater. Chem. A 4 (2016) 529–536.
[40] Y. Khabzina, D. Farrusseng, Microporous Mesoporous Mater. 265 (2018) 143–148.
[41] Y. Cai, A.R. Kulkarni, Y. Huang, et al., Cryst. Growth Des. 14 (2014) 6122–6128.
[42] S. Rong, P. Su, S. Chen, et al., Chin. Chem. Lett. 33 (2022) 2134–2138.
[43] Y. Cai, Y. Zhang, Y. Huang, et al., Cryst. Growth Des. 12 (2012) 3709–3713.
[44] B. Seoane, C. Téllez, J. Coronas, et al., Sep. Purif. Technol. 111 (2013) 72–81.
[45] L. Li, Y. Wang, J. Yang, et al., ChemPlusChem 81 (2016) 222–228.
[46] Y. Cheng, Q. Feng, M. Yin, et al., Tetrahedron Lett. 57 (2016) 3814–3818.
[47] Y. Li, S. Li, Y. Jiang, et al., Chem. Commun. 54 (2018) 9789–9792.